37th AIAA Fluid Dynamics Conference and Exhibit
25 - 28 June 2007, Miami, FL

AIAA 2007-4120

The Taylor Profile in Porous Channels with Arbitrary Headwall Injection

Tony Saad* and Joseph Majdalani†
University of Tennessee Space Institute, Tullahoma, TN 37388

In a recent study, Taylor's incompressible and rotational core flow in a cylindrical porous chamber was extended by the authors to account for arbitrary headwall injection. In this study, we construct the solution for the two-dimensional planar case while incorporating variable headwall injection. The resulting representation is especially well suited to model the non-reactive gaseous motion in slab hybrid rockets and in two-dimensional channels with porous walls. Our analysis employs Euler's steady-state equations from which an approximate solution is derived. The mean flow approximation that ensues satisfies the no slip boundary condition at the walls. It is confirmed through comparisons with numerical simulations evolving from a pressure-based finite volume solver. The analytical solutions are compared to the numerical results under inviscid flow conditions. Interestingly, they become exact at the wall and along the midsection plane where the error in the approximations vanishes identically. Furthermore, our solutions become increasingly more accurate in the downstream direction. The final formulations enable us to approximate the flowfield in both hybrid and solid rockets with variable headwall injection patterns.

Nomenclature

$2a$	= total channel height
$\boldsymbol{u}$	= normalized velocity $(\bar{u}_x, \bar{u}_y)/U_w$
U_c	= uniform headwall injection velocity, $\bar{u}_x(0,\bar{y})$
u_c	= normalized headwall injection velocity, U_c/U_w
U_w	= sidewall injection velocity, $-\bar{u}_y(a,\bar{y})$
x, y	= normalized axial and transverse coordinates, $\bar{x}/a$, $\bar{y}/a$

Greek

ν	= kinematic viscosity, μ/ρ
ρ	= density

Subscripts and Symbols

c	= centerline property
h, w	= property at headwall or sidewall
x	= axial (streamwise) component
y	= transverse (wall-normal) component
$\bar{}$	= overbars denote dimensional variables

I. Introduction

TAYLOR's simple analytical solution for describing the gaseous motion in solid rocket motors (SRMs) was obtained under the contingencies of steady, incompressible, rotational, axisymmetric, and quasi-viscous flow.[1] Despite being inviscid, its streamlines observed the no slip requirement along the porous sidewall.[2] In recent work, Majdalani and Saad[3] presented a closed-form inviscid solution for the axisymmetric Taylor-Culick flow with

*Doctoral Research Assistant, Department of Mechanical, Aerospace and Biomedical Engineering. Member AIAA.
†Jack D. Whitfield Professor of High Speed Flows, Department of Mechanical, Aerospace and Biomedical Engineering. Member AIAA. Fellow ASME.

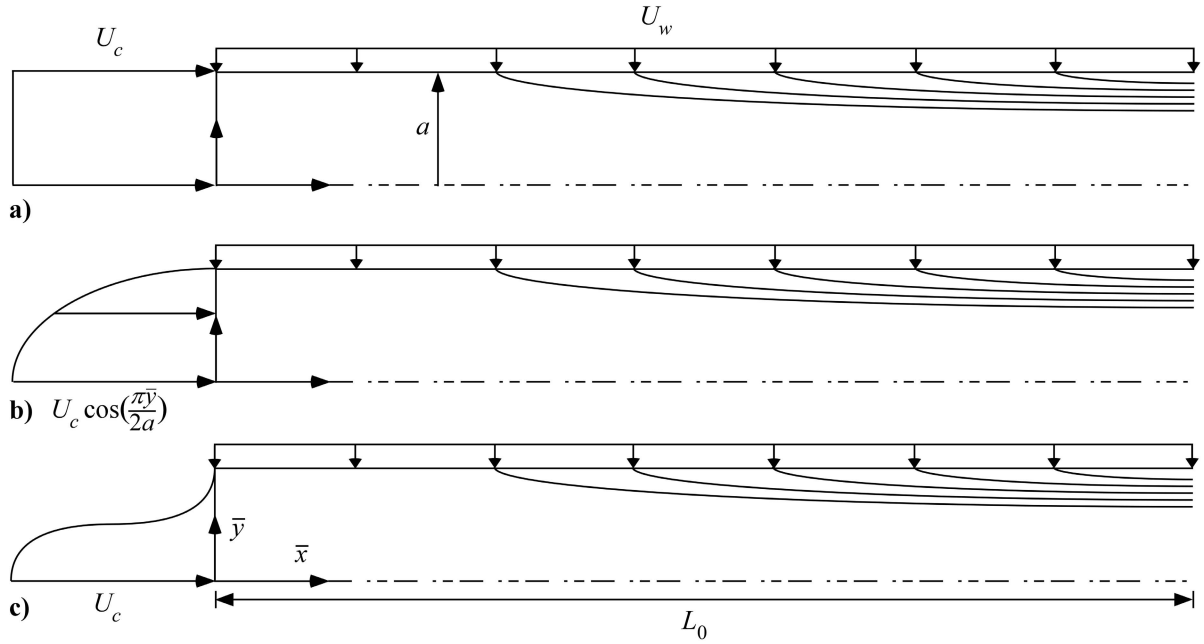

Figure 1. Sketch of a porous channel with a) uniform, b) Berman's half cosine and c) arbitrary headwall injection.

arbitrary headwall injection; their model was suitable for describing the bulk fluid motion in a porous cylinder. In this article, we investigate the two-dimensional porous channel with variable headwall injection. Obtaining an analytical model for the Cartesian case not only adds to our armory of approximations for mean flowfields but also carries the advantage of providing an avenue for comparison with experimental and numerical studies of slab burner grains in both hybrid and solid rocket systems. These configurations are becoming increasingly more popular among academicians and research-development teams, not only in reactive flow investigations but also in technological applications involving flow through porous media, starting with the original Taylor solution itself (Taylor[2]). Examples abound as a large number of investigations have already been carried out in two-dimensional settings. To cite a few, one may enumerate, in reverse chronological order: Fischbach *et al.*;[4] Féraille and Casalis;[5] Fabignon *et al.*;[6] Chu *et al.*;[7] Najjar *et al.*;[8] Griffond;[9] Apte and Yang;[10,11] Griffond and Casalis;[12,13] Venugopal *et al.*;[14,15] Ugurtas;[16] Couton *et al.*;[17] Lupoglazoff and Vuillot;[18] Balakrishnan *et al.*;[19] Ma *et al.*;[20,21] Watson *et al.*;[22] and lastly, perhaps one of the most influential in its category, is the 1986 paper by Traineau *et al.*[23] The geometric and physical parameters utilized in Traineau's experimental and theoretical work are later adopted by several capable researchers such as Balakrishnan *et al.*,[19] Venugopal *et al.*,[14,15] and Apte and Yang.[10,11] Their analysis is also used as a baseline in the compressible flow studies conducted by Maicke and Majdalani.[24]

Overall, our solution is intended to offer a basic cold flow model for both solid and hybrid slab rockets. Since the porous channel flow has been proven to provide a reliable approximation for the core flowfield in a slab rocket, it can be employed in a multitude of studies seeking to examine (a) internal rocket gas dynamics, (b) flow instability, (c) particle-mean flow interactions, and (d) fluid-structure interactions. Other technological applications of the two-dimensional flow with sidewall mass injection include: (i) surface transpiration, (ii) film cooling, (iii) filtration, and (iv) isotope separation. For the solid rocket motor, the headwall-to-sidewall injection velocity ratio will be shown to be of order unity; however, it is one to two orders of magnitude larger for hybrids. Being around 100 and above, the relatively large headwall injection ratio associated with hybrid rocket faceplates leads to the onset of a distinct streamtube motion that permeates the vast portion of the chamber. For this reason, our analysis is carried out under incompressible, inviscid, and non-reactive conditions. Further refinements to our first order approximation will be deferred to later work.

The paper is organized as follows. The mathematical model is first defined along with the relevant boundary conditions. Subsequently, a general solution for an arbitrary headwall injection profile is derived. This is followed by special applications commensurate with uniform, Berman's half cosine, Poiseuille, and turbulent injection profiles. Finally, a numerical comparison with inviscid flow simulations is described.

II. Mathematical Model

The slab motor can be idealized as a two-dimensional channel of porous length L_0 and height $2a$ with both a 'reactive' headwall and a nozzleless aft end (see Fig. 1). At the headwall, a fluid stream (which may denote an oxidizer or gaseous propellant mixture) is injected into the chamber at an axially uniform speed U_c. This incoming stream must be assimilated with the lateral crossflow sustained by uniform mass addition at the porous sidewall. Naturally, the sidewall injection velocity U_w is commensurate with the solid propellant or fuel regression rates. In hybrids, U_w can be appreciably smaller than U_c due to slow fuel pyrolysis, whereas these two values will be the same in SRM analysis. As shown in Fig. 1, $\bar{x}$ and $\bar{y}$ stand for the axial and normal coordinates used to describe the position from the headwall to the typical nozzle attachment point at the aft boundary. In the event that the fuel or solid propellant burning rate is not uniform along the sidewall, the sidewall injection velocity can be estimated from the average value

$$U_w = -\frac{1}{L_0}\int_0^{L_0} \bar{u}_y(\bar{x}, a)\,\mathrm{d}\bar{x} \tag{1}$$

A. Normalization

For the sake of convenience, we begin by normalizing principal variables and operators. This can be done by setting [25]

$$x = \frac{\bar{x}}{a};\ y = \frac{\bar{y}}{a};\ \nabla = a\bar{\nabla};\ p = \frac{\bar{p}}{\rho U_w^2};\ \psi = \frac{\bar{\psi}}{aU_w} \tag{2}$$

$$u_x = \frac{\bar{u}_x}{U_w};\ u_y = \frac{\bar{u}_y}{U_w};\ \boldsymbol{\Omega} = \frac{\bar{\boldsymbol{\Omega}}a}{U_w};\ u_c = \frac{U_c}{U_w};\ L = \frac{L_0}{a} \tag{3}$$

Here $U_c = \bar{u}_x(0,0)$ and $U_w = -\bar{u}_y(\bar{x}, a)$ allude to the uniform fluid injection velocities along the headwall and sidewall, respectively. For steady inviscid motion, the vorticity transport equation reduces to

$$\nabla \times \boldsymbol{u} \times \boldsymbol{\Omega} = 0\ ;\quad \boldsymbol{\Omega} = \nabla \times \boldsymbol{u} \tag{4}$$

To reduce redundant boundary conditions, we consider half of the channel and utilize symmetry about the midsection plane. This enables us to write

$$\begin{cases} u_y(x,0) = 0 & \text{(no flow across midsection plane)} \\ u_x(0,y) = u_0(y) & \text{(headwall injection profile)} \\ u_y(x,1) = -1 & \text{(constant sidewall mass addition)} \\ u_x(x,1) = 0 & \text{(no slip)} \end{cases} \tag{5}$$

B. Vorticity-Stream Function Formulation

Continuity is fulfilled by the stream function when it is written as

$$u_x = \frac{\partial \psi}{\partial y} \qquad u_y = -\frac{\partial \psi}{\partial x} \tag{6}$$

Acknowledging that vorticity has a single non-zero component, viz.

$$\Omega_x = \Omega_y = 0;\quad \Omega_z = \frac{\partial u_y}{\partial x} - \frac{\partial u_x}{\partial y} \tag{7}$$

we obtain

$$\nabla^2 \psi = -\Omega_z \tag{8}$$

As usual, the next step is to substitute into the vorticity transport equation given by Eq. (4). Its fulfillment beckons a functional relation for Ω_z of the form

$$\Omega = \Omega_z = F(\psi) \quad \text{since} \quad \frac{(\Omega_z)_x}{(\Omega_z)_y} = \frac{[F(\psi)]_x}{[F(\psi)]_y} = \frac{F_\psi \psi_x}{F_\psi \psi_y} = \frac{\psi_x}{\psi_y} \tag{9}$$

A useful choice can be shown to be

$$\Omega = C^2 \psi \tag{10}$$

Despite the non-uniqueness of this relation, it leads to a model that permits the assimilation of the four boundary conditions in Eq. (5). In fact, straightforward substitution into Eq. (8) yields the standard Helmholtz type equation,

$$\frac{\partial^2 \psi}{\partial x^2} + \frac{\partial^2 \psi}{\partial y^2} + C^2 \psi = 0 \tag{11}$$

When written in terms of the stream function, our boundary conditions translate into

$$\frac{\partial \psi(x,0)}{\partial x} = 0 \quad \text{(a)}; \quad \frac{\partial \psi(x,1)}{\partial y} = 0 \quad \text{(b)}; \quad \frac{\partial \psi(x,1)}{\partial x} = 1 \quad \text{(c)}; \quad \frac{\partial \psi(0,y)}{\partial y} = u_0(y) \quad \text{(d)}; \tag{12}$$

A general solution for Eq. (11) may be obtained straightforwardly using separation of variables; the result is

$$\psi(x,y) = (\alpha x + \beta)[A\cos(Cy) + B\sin(Cy)] \tag{13}$$

We note that, by linearity, any combination of equations akin to Eq. (13) is also a solution to Eq. (11).

III. General Solution

Implementation of the four constraints may be systematically carried out, preferably in the order in which they appear. For instance, Eq. (12)a gives:

$$\frac{\partial \psi(x,0)}{\partial x} = \alpha A\cos(Cy) + \alpha B\sin(Cy)\big|_{y=0} = 0 \tag{14}$$

This implies that $A = 0$. Without loss of generality, we set $B = 1$ and rewrite Eq. (12)b as

$$\frac{\partial \psi}{\partial y}(x,1) = C(\alpha x + \beta)\cos(C) = 0 \quad \text{or} \quad C_n = (n + \tfrac{1}{2})\pi \quad \forall n \in \{0,1,2,3,...,\infty\} \tag{15}$$

The ensuing eigenfunctions take the form

$$\psi_n = (\alpha_n x + \beta_n)\sin\left[\left(n + \tfrac{1}{2}\right)\pi y\right] \tag{16}$$

Using $C_n = \left(n + \tfrac{1}{2}\right)\pi$ enables us to sum over eigenfunctions that alternate between wall suction and injection. The general solution can be obtained by superposition. We therefore put

$$\psi(x,y) = \sum_{n=0}^{\infty} (\alpha_n x + \beta_n)\sin\left[\left(n + \tfrac{1}{2}\right)\pi y\right] \tag{17}$$

A. Taylor-Type Solutions

At this juncture, we can resume implementing the problem's constraints. Forthwith, boundary condition (12)c yields

$$\frac{\partial \psi}{\partial x}(x,1) = \sum_{n=0}^{\infty} \alpha_n \sin\left[\left(n + \tfrac{1}{2}\right)\pi\right] = 1 \quad \text{or} \quad \sum_{n=0}^{\infty} (-1)^n \alpha_n = 1 \tag{18}$$

Several different solutions may hence exist depending on the choice of α_n. Here, we shall focus on the case leading to Taylor's. From the many solutions that conform to Eq. (18), Taylor's planar solution may be uniquely recovered by setting

$$\alpha_0 = 1 \quad \text{and} \quad \alpha_n = 0; \forall n \neq 0 \tag{19}$$

The last headwall boundary condition renders

$$\frac{\partial \psi}{\partial y}(0,y) = \tfrac{1}{2}\pi \sum_{n=0}^{\infty} (2n+1)\beta_n \cos\left[\left(n + \tfrac{1}{2}\right)\pi y\right] = u_0(y) \tag{20}$$

Orthogonality may then be invoked to retrieve β_n; one recovers

$$\beta_n \int_0^1 (2n+1)\cos^2[(n+\tfrac{1}{2})\pi y]\,\mathrm{d}y = (2/\pi)\int_0^1 u_0(y)\cos[(n+\tfrac{1}{2})\pi y]\,\mathrm{d}y \tag{21}$$

or

$$\beta_n = \frac{4}{(2n+1)\pi}\int_0^1 u_0(y)\cos[(n+\tfrac{1}{2})\pi y]\,\mathrm{d}y \tag{22}$$

The extended Taylor solution is thus at hand. From Eq. (17) one can put

$$\psi(x,y) = x\sin\left(\tfrac{1}{2}\pi y\right) + \sum_{n=0}^{\infty} \beta_n \sin\left[\left(n + \tfrac{1}{2}\right)\pi y\right] \tag{23}$$

where

$$\beta_n = \begin{cases} \dfrac{8(-1)^n u_c}{\pi^2 (2n+1)^2}; & u_0 = u_c \\ \dfrac{2u_c}{\pi};\ n=0 \quad (0;\ \forall n \neq 0); & u_0 = u_c \cos\left(\tfrac{1}{2}\pi y\right) \\ \dfrac{64(-1)^n u_c}{\pi^4 (2n+1)^4}; & u_0 = u_c\left(1-y^2\right) \\ \dfrac{1792(-1)^n u_c}{\pi^{10}(2n+1)^{10}}\begin{bmatrix} -46080 + 5760\pi^2(2n+1)^2 \\ -120\pi^4(2n+1)^4 + \pi^6(2n+1)^6 \end{bmatrix}; & u_0 = u_c\left(1-y^8\right) \end{cases} \tag{24}$$

Corresponding axial and normal velocities emerge as

$$u_x(x,y) = \tfrac{1}{2}\pi x \cos\left(\tfrac{1}{2}\pi y\right) + \tfrac{1}{2}\pi \sum_{n=0}^{\infty} (2n+1)\beta_n \cos\left[\left(n+\tfrac{1}{2}\right)\pi y\right];\quad u_y(x,y) = -\sin\left(\tfrac{1}{2}\pi y\right) \tag{25}$$

Similarly, the vorticity takes the form

$$\Omega_z = \tfrac{1}{4}\pi^2 x \sin\left(\tfrac{1}{2}\pi y\right) + \tfrac{1}{4}\pi^2 \sum_{n=0}^{\infty} (2n+1)^2 \beta_n \sin\left[\left(n+\tfrac{1}{2}\right)\pi y\right] \tag{26}$$

Based on Eq. (22), specific solutions may be secured for various inlet profiles. Here we consider those corresponding to uniform injection, Berman's half cosine, Poiseuille's, and turbulent flow. These are posted in Table 1. For a simulated hybrid rocket, the centerline velocities of arbitrary profiles required to produce the same flux at $x = 0$ as that of a uniform injection can be extracted from a mass balance

$$\int_{-1}^{1} u_0(y)\,dy = \int_{-1}^{1} u_c\,dy = 2 \tag{27}$$

The equivalent centerline velocities for Berman's half cosine, Poiseuille's, and turbulent flow profiles of the type $u_c\left(1-y^m\right)$ are found to be

$$u_c = \begin{cases} \tfrac{1}{2}\pi \\ \tfrac{3}{2} \\ \dfrac{2(m+1)}{1-(-1)^m + 2m} \end{cases} \tag{28}$$

Note that the third member of Eq. (28) will reproduce the Poiseuille case of $u_c = \frac{3}{2}$ for $m = 2$. Plots of the vorticity contours are shown in Fig. 2 for Berman's half cosine, Poiseuille, and power law profiles. Note that in the case of uniform injection, the vorticity is restricted to a narrow region near the sidewall because the flow is essentially irrotational, being nearly uniform inside the chamber.

B. Pressure Analysis

The pressure distribution can be easily obtained from $\boldsymbol{u}\cdot\nabla\boldsymbol{u} = -\nabla p$ by integrating in two spatial directions and adding the results. At the outset, one obtains

$$p = p_0 - \tfrac{1}{2}\boldsymbol{u}\cdot\boldsymbol{u} - \int u_y \frac{\partial u_x}{\partial y}\mathrm{d}x - \int u_x \frac{\partial u_y}{\partial x}\mathrm{d}y = p_0 - \tfrac{1}{2}\boldsymbol{u}\cdot\boldsymbol{u} - \int u_y \frac{\partial u_x}{\partial y}\mathrm{d}x \ \text{ when } u_y \neq u_y(x) \tag{29}$$

Table 1. Solutions for three different headwall injection profiles

$u_0(y)$	$\psi(x,y)$	$u_x(x,y)$
u_c	$x\sin\left(\frac{1}{2}\pi y\right) + 8u_c\sum_{n=0}^{\infty}\frac{(-1)^n}{\pi^2(2n+1)^2}\sin\left[\left(n+\frac{1}{2}\right)\pi y\right]$	$\frac{1}{2}\pi x\cos\left(\frac{1}{2}\pi y\right) + 4u_c\sum_{n=0}^{\infty}\frac{(-1)^n}{\pi(2n+1)}\cos\left[\left(n+\frac{1}{2}\right)\pi y\right]$
$u_c\cos(\frac{1}{2}\pi y)$	$(x + 2u_c/\pi)\sin\left(\frac{1}{2}\pi y\right)$	$\frac{1}{2}\pi(x + 2u_c/\pi)\cos\left(\frac{1}{2}\pi y\right)$
$u_c(1-y^2)$	$x\sin\left(\frac{1}{2}\pi y\right) + 64u_c\sum_{n=0}^{\infty}\frac{(-1)^n}{\pi^4(2n+1)^4}\sin\left[\left(n+\frac{1}{2}\right)\pi y\right]$	$\frac{1}{2}\pi x\cos\left(\frac{1}{2}\pi y\right) + 32u_c\sum_{n=0}^{\infty}\frac{(-1)^n}{\pi^3(2n+1)^3}\cos\left[\left(n+\frac{1}{2}\right)\pi y\right]$

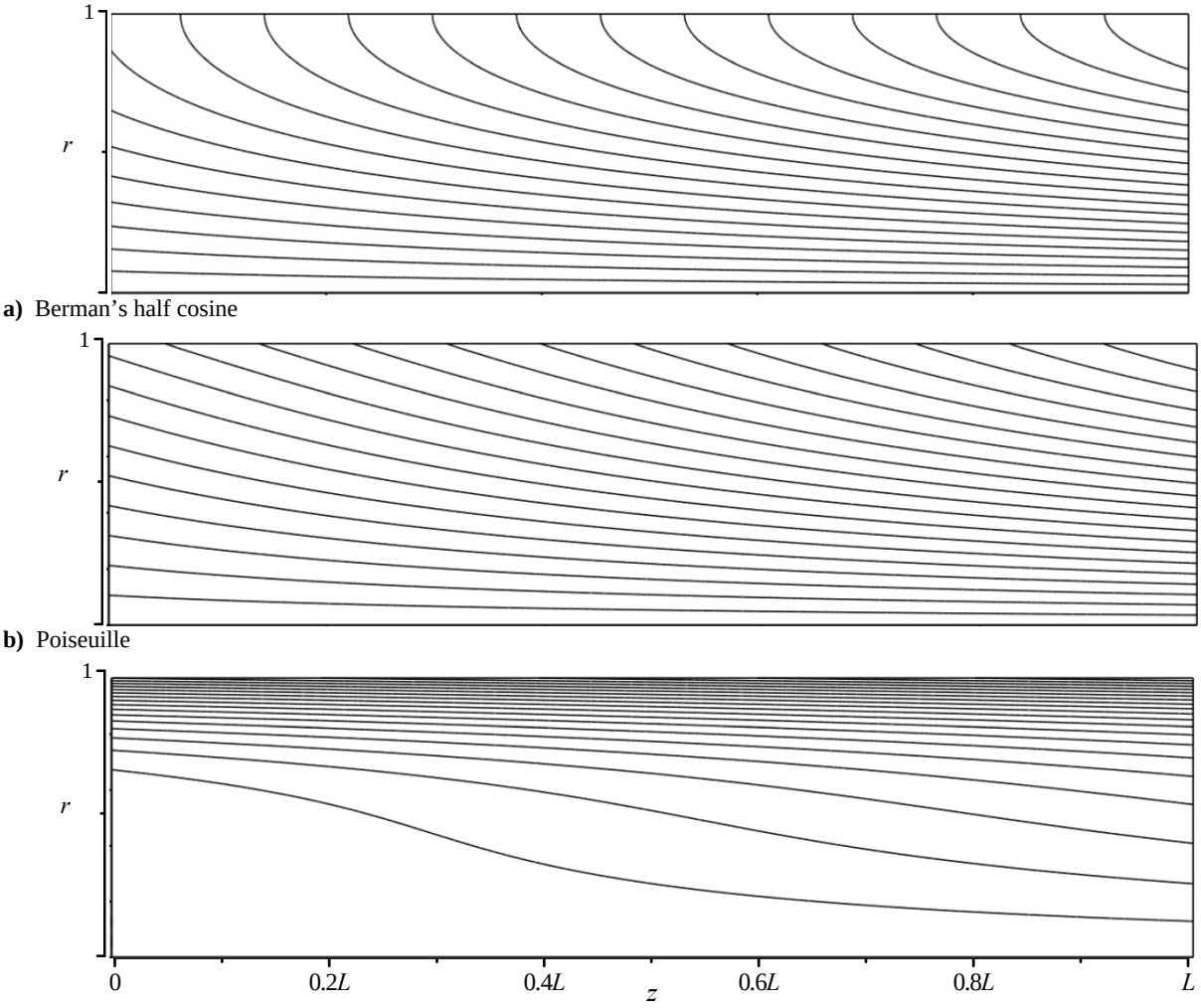

a) Berman's half cosine

b) Poiseuille

c) turbulent power law

Figure 2. Vorticity contours for a) Berman's half cosine, b) Poiseuille, and c) power law injection profiles. All plots are for $u_c = 1$.

where $p_0 = p(0,0)$. The pressure and vorticity distributions resulting from several injection profiles are given in Table 2. The remaining profiles lead to lengthy expressions that are best relegated to a symbolic code.

Table 2. Vorticity and pressure distributions for several headwall injection profiles

$u_0(y)$	$\Omega(x,y)$	$p(x,y)$
u_c	$\frac{1}{4}\pi^2 x\sin\left(\frac{1}{2}\pi y\right) + 2u_c\sum_{n=0}^{\infty}(-1)^n\sin\left[\left(n+\frac{1}{2}\right)\pi y\right]$	$p_0 - \frac{1}{2}\left(\frac{1}{4}\pi^2x^2+1\right)\sin^2\left(\frac{1}{2}\pi y\right)$ $-\frac{2}{\pi}\left[u_c\left(\tan^{-1}e^{-\frac{1}{2}i\pi y}+\tan^{-1}e^{\frac{1}{2}i\pi y}\right)+\frac{1}{4}\pi^2 x\cos\left(\frac{1}{2}\pi y\right)\right]^2$
$u_c\cos(\frac{1}{2}\pi y)$	$\frac{1}{4}\pi^2\sin\left(\frac{1}{2}\pi y\right)\left(x+2\frac{u_c}{\pi}\right)$	$p_0 - \frac{1}{4}\left[\frac{1}{2}\pi^2x^2 + 2\pi u_c x + \left(u_c^2-1\right)\cos\left(\pi y\right)+u_c^2+1\right]$
$u_c(1-y^2)$	$\frac{1}{4}\pi^2 x\sin\left(\frac{1}{2}\pi y\right)+16u_c\sum_{n=0}^{\infty}\frac{(-1)^n}{\pi^2(2n+1)^2}\sin\left[\left(n+\frac{1}{2}\right)\pi y\right]$	

C. Nonlinear Residual in the Vorticity Transport Equation

For each eigensolution given by Eq. (16), the vorticity transport equation is satisfied (i.e. Eq. (4)) and the residual error Q_n is identically zero:

$$Q_n(x,y) = \frac{\partial \psi_n}{\partial x}\frac{\partial \Omega_n}{\partial y} - \frac{\partial \psi_n}{\partial y}\frac{\partial \Omega_n}{\partial x} = C_n^2 \frac{\partial \psi_n}{\partial x}\frac{\partial \psi_n}{\partial y} - C_n^2 \frac{\partial \psi_n}{\partial y}\frac{\partial \psi_n}{\partial x} = 0 \tag{30}$$

where

$$\Omega = \Omega_z = C_n^2 \psi_n; \quad C_n = (n + \tfrac{1}{2})\pi \tag{31}$$

When Eq. (30) is summed over all eigenmodes, it remains zero. This represents an interesting situation, albeit hypothetical, for which the eigensolutions coexist with no interaction. However, when coupling between the eigenmodes is considered, the total vorticity and stream function, given by Eq. (17), must be substituted into Eq. (4). The cumulative error becomes

$$Q(x,y) = \frac{\partial \psi}{\partial x}\frac{\partial \Omega}{\partial y} - \frac{\partial \psi}{\partial y}\frac{\partial \Omega}{\partial x} = \sum_{n=0}^{m}\frac{\partial \psi_n}{\partial x}\sum_{n=0}^{m}\frac{\partial \Omega_n}{\partial y} - \sum_{n=0}^{m}\frac{\partial \psi_n}{\partial y}\sum_{n=0}^{m}\frac{\partial \Omega_n}{\partial x} \tag{32}$$

where

$$\begin{aligned} \frac{\partial \psi_n}{\partial x} &= \alpha_n \sin(C_n y); & \frac{\partial \Omega_n}{\partial x} &= C_n^2 \frac{\partial \psi_n}{\partial x} \\ \frac{\partial \psi_n}{\partial y} &= C_n(\alpha_n x + \beta_n)\cos(C_n y); & \frac{\partial \Omega_n}{\partial y} &= C_n^2 \frac{\partial \psi_n}{\partial y} \end{aligned} \tag{33}$$

If we further take into account that

$$\alpha_0 = 1 \quad \text{and} \quad \alpha_n = 0; \forall n \neq 0 \tag{34}$$

then Eq. (32) simplifies to

$$Q(y) = \frac{\partial \psi_0}{\partial x}\sum_{n=0}^{m}\left(C_n^2 - C_0^2\right)\frac{\partial \psi_n}{\partial y} \tag{35}$$

Equation (35) represents the error in the vorticity transport equation due to nonlinear coupling. In general, it is not zero except in the case of self-similar headwall injection profiles such as Berman's. Based on the solution given by Eqs. (16) and (19), the Taylor-type flow (for which $\alpha_0 = 1$ and $\alpha_n = 0; \forall n \neq 0$) will incur a residual amounting to

$$Q(y) = \sin\left(\tfrac{1}{2}\pi y\right)\sum_{n=1}^{m}\left(C_n^2 - C_0^2\right)C_n \beta_n \cos(C_n y) \tag{36}$$

Note that the residual is identically zero in the midsection plane and along the chamber walls irrespective of the assumed injection profile. Moreover, being independent of the axial position, the residual becomes proportionately smaller in long porous channels such as those associated with rocket chambers. These factors may explain the surprising accuracy of the present approximation for several case studies that are described in the next section.

IV. Numerical Verification

By way of verification, we present a numerical solution for the inviscid flow equations using several headwall injection profiles. The simulations are carried out using a two dimensional finite volume code. These are based on a chamber with an average sidewall velocity of 10 m/s and purely inviscid conditions. The aspect ratio is chosen to be L = 16 while the actual length of the domain is 1.6 m×0.1 m; it is finely meshed into 589,824 equally spaced control volumes (3,072×192). A first order upwind scheme is used for spatial discretization while the SIMPLE algorithm is used to resolve pressure-velocity coupling. The boundary conditions at the sidewall are specified as velocity inlets to closely mimic the mathematical model where injection is imposed uniformly along the grain surface. The headwall is also specified as an inlet. On the right-hand-side of the domain, a pressure outlet boundary condition is prescribed. Although an outflow boundary condition can also be imposed at the downstream section, it is discounted here to avoid the possible case of partially developed flow. The difference between an outflow and a pressure outlet boundary condition is that, in the latter case, the exit pressure is fixed at the boundary. Finally, the working fluid is taken to be air at standard conditions.

The results of our inviscid simulations are shown in Figs. 3-4 using several injection profiles. In Fig. 3, the evolution of the flowfield is depicted in the forward segment of the chamber where the curves are located at x/L = 0, 0.1, 0.2, 0.3 and 0.4. Note that the agreement with numerics improves with further development of the flowfield and is most remarkable for Berman's half-cosine and Poiseuille's profiles. This may be attributed to our formulation

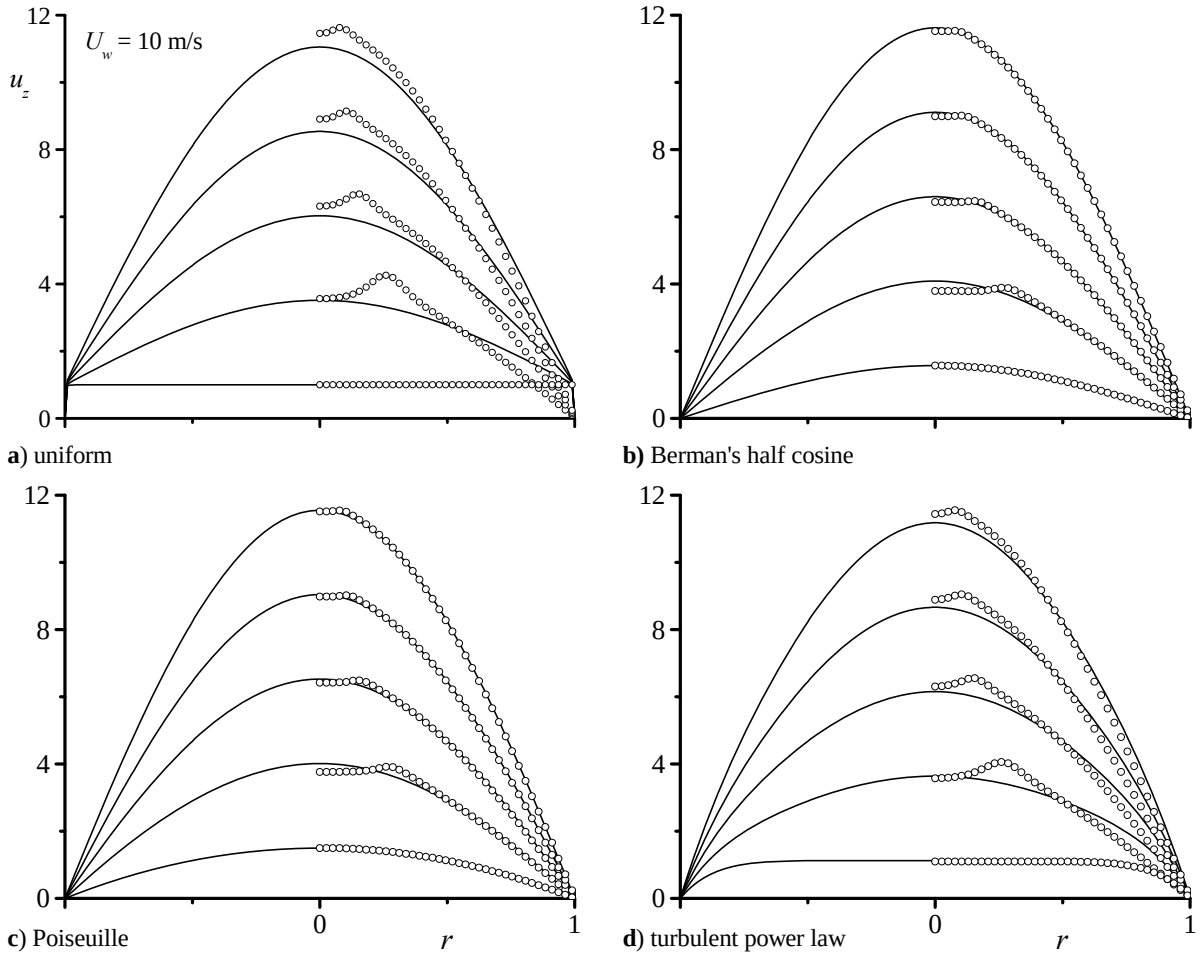

Figure 3. Comparison between analytical (solid lines) and numerical simulations (circles) using a) uniform, b) half cosine, c) parabolic, and d) turbulent profiles. Identical inviscid conditions are set in both numerical and analytical models using headwall injection constants of $u_c = 1, \frac{1}{2}\pi, \frac{3}{2}, \frac{9}{8}$, and *x/L* = 0, 0.1, 0.2, 0.3 and 0.4.

being exact for Berman's case and to Poiseuille's profile being the one from our group of test cases that most closely resembles that of Berman's. The least agreement corresponds to the uniform profile which poses a discontinuity at the walls at the start of the simulations. In Fig. 4, the streamwise evolution of both axial and transverse velocities is illustrated along the length of the chamber. The agreement between the analytical solutions and numerical simulations is seen to be excellent when the flow becomes essentially fully developed. Despite the comparison being limited in scope, it reaffirms the viability of the analytical approximations derived in Sec. III.

V. Conclusions

In this study, we derive approximate solutions for the inviscid incompressible Taylor flow in a two-dimensional porous channel with arbitrary headwall injection. The solutions can be considered to be quasi-viscous as they fully secure the no-slip boundary condition at the walls. This is especially true for the hybrid model in which the large headwall injection velocity offsets the secondary cross-flow effect caused by small sidewall injection at the fore end corner points. The known singularity in the planar Taylor flow at $x = 0$ is thereby mitigated in the hybrid representation (i.e., for large headwall-to-sidewall injection). Furthermore, provided that headwall mass addition is properly accounted for, the effect of varying the headwall injection rate is found to be negligible in sufficiently long slab rocket motors. Through the present analysis, we gain further confidence in the validity of the inviscid representation after comparing the analytical solution to numerical computations. In future work, we hope to explore the existence of other possible solutions with varying levels of energies. We also hope to construct an asymptotic viscous solution for the Taylor flow with arbitrary headwall injection.

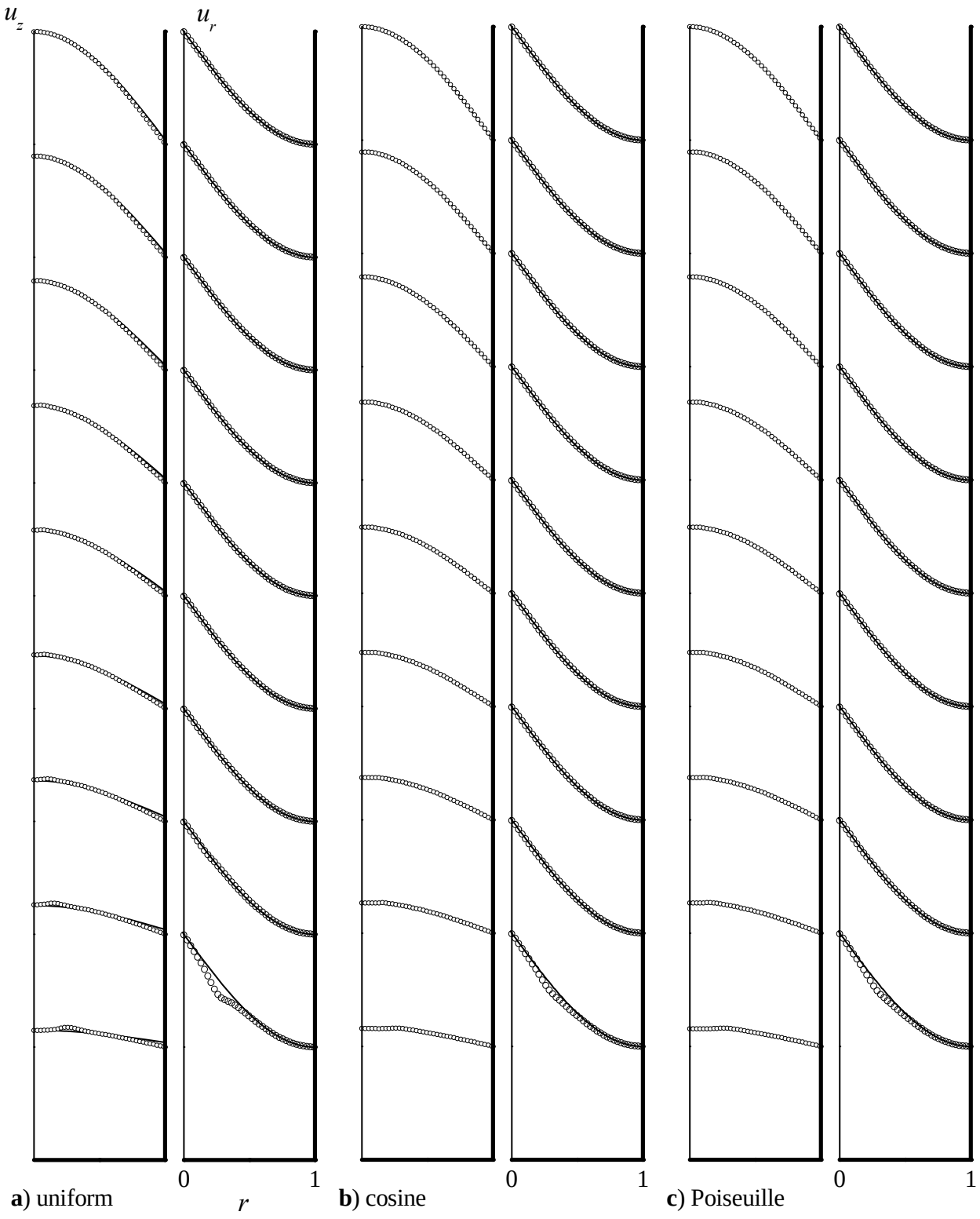

Figure 4. Comparison between analytical (solid lines) and numerical simulations (circles) for a porous channel using a) uniform, b) half cosine, and c) parabolic injection profiles. The corresponding headwall injection constants are $u_c = 1, \frac{1}{2}\pi,$ and $\frac{3}{2}$, respectively.

Acknowledgments

This work is sponsored by the National Science Foundation. The second author acknowledges valuable discussions with Dr. Grégoire Casalis, Professor and Director of the Doctoral School of Aeronautics and Astronautics, SUPAERO, and Research Director, Department of Aerodynamics and Energetics, ONERA, Toulouse, France.

References

[1]Culick, F. E. C., "Rotational Axisymmetric Mean Flow and Damping of Acoustic Waves in a Solid Propellant Rocket," *AIAA Journal,* Vol. 4, No. 8, 1966, pp. 1462-1464.

[2]Taylor, G. I., "Fluid Flow in Regions Bounded by Porous Surfaces," *Proceedings of the Royal Society, London, Series A,* Vol. 234, No. 1199, 1956, pp. 456-475.

[3]Majdalani, J., and Saad, T., "The Taylor-Culick Profile with Arbitrary Headwall Injection," *Physics of Fluids,* Vol. 19, No. 6, 2007.

[4]Fischbach, S. R., Majdalani, J., and Flandro, G. A., "Acoustic Instability of the Slab Rocket Motor," *Journal of Propulsion and Power,* Vol. 23, No. 1, 2007, pp. 146-157.

[5]Féraille, T., and Casalis, G., "Channel Flow Induced by Wall Injection of Fluid and Particles," *Physics of Fluids,* Vol. 15, No. 2, 2003, pp. 348-360.

[6]Fabignon, Y., Dupays, J., Avalon, G., Vuillot, F., Lupoglazoff, N., Casalis, G., and Prévost, M., "Instabilities and Pressure Oscillations in Solid Rocket Motors," *Journal of Aerospace Science and Technology,* Vol. 7, No. 3, 2003, pp. 191-200.

[7]Chu, W.-W., Yang, V., and Majdalani, J., "Premixed Flame Response to Acoustic Waves in a Porous-Walled Chamber with Surface Mass Injection," *Combustion and Flame,* Vol. 133, No. 6129, 2003, pp. 359-370.

[8]Najjar, F. M., Haselbacher, A., Ferry, J. P., Wasistho, B., Balachandar, S., and Moser, R., "Large-Scale Multiphase Large-Eddy Simulation of Flows in Solid-Rocket Motors," AIAA Paper 2003-3700, June 2003.

[9]Griffond, J., "Receptivity and Aeroacoustic Resonance in Channels with Blowing Walls," *Physics of Fluids,* Vol. 14, No. 11, 2002, pp. 3946-3962.

[10]Apte, S., and Yang, V., "Unsteady Flow Evolution in a Porous Chamber with Surface Mass Injection. Part II: Acoustic Excitation," *AIAA Journal,* Vol. 40, No. 2, 2002, pp. 244-253.

[11]Apte, S., and Yang, V., "Unsteady Flow Evolution in a Porous Chamber with Surface Mass Injection. Part I: Free Oscillation," *AIAA Journal,* Vol. 39, No. 8, 2001, pp. 1577-1586.

[12]Griffond, J., and Casalis, G., "On the Nonparallel Stability of the Injection Induced Two-Dimensional Taylor Flow," *Physics of Fluids,* Vol. 13, No. 6, 2001, pp. 1635-1644.

[13]Griffond, J., and Casalis, G., "On the Dependence on the Formulation of Some Nonparallel Stability Approaches Applied to the Taylor Flow," *Physics of Fluids,* Vol. 12, No. 2, 2000, pp. 466-468.

[14]Venugopal, P., Najjar, F. M., and Moser, R. D., "Numerical Simulations of Model Solid Rocket Motor Flows," AIAA Paper 2001-3950, July 2001.

[15]Venugopal, P., Najjar, F. M., and Moser, R. D., "DNS and LES Computations of Model Solid Rocket Motors," AIAA Paper 2000-3571, July 2000.

[16]Ugurtas, B., Avalon, G., Lupoglazoff, N., Vuillot, F., and Casalis, G., "Stability and Acoustic Resonance of Internal Flows Generated by Side Injection," *Solid Propellant Chemistry, Combustion, and Motor Interior Ballistics*, Vol. 185, edited by V. Yang, T. B. Brill, and W.-Z. Ren, AIAA Progress in Astronautics and Aeronautics, Washington, DC, 2000, pp. 823-836.

[17]Couton, D., Doan-Kim, S., and Vuillot, F., "Numerical Simulation of Vortex-Shedding Phenomenon in a Channel with Flow Induced through Porous Wall," *International Journal of Heat and Fluid Flow,* Vol. 18, No. 3, 1997, pp. 283-296.

[18]Lupoglazoff, N., and Vuillot, F., "Numerical Simulation of Vortex Shedding Phenomenon in Two-Dimensional Test Case Solid Rocket Motors," AIAA Paper 92-0776, January 1992.

[19]Balakrishnan, G., Liñan, A., and Williams, F. A., "Compressible Effects in Thin Channels with Injection," *AIAA Journal,* Vol. 29, No. 12, 1991, pp. 2149-2154.

[20]Ma, Y., Van Moorhem, W. K., and Shorthill, R. W., "Experimental Investigation of Velocity Coupling in Combustion Instability," *Journal of Propulsion and Power,* Vol. 7, No. 5, 1991, pp. 692-699.

[21]Ma, Y., Van Moorhem, W. K., and Shorthill, R. W., "Innovative Method of Investigating the Role of Turbulence in the Velocity Coupling Phenomenon," *Journal of Vibration and Acoustics-Transactions of the ASME,* Vol. 112, No. 4, 1990, pp. 550-555.

[22]Watson, E. B. B., Banks, W. H. H., Zaturska, M. B., and Drazin, P. G., "On Transition to Chaos in Two-Dimensional Channel Flow Symmetrically Driven by Accelerating Walls," *Journal of Fluid Mechanics,* Vol. 212, No. 1, 1990, pp. 451-485.

[23]Traineau, J. C., Hervat, P., and Kuentzmann, P., "Cold-Flow Simulation of a Two-Dimensional Nozzleless Solid-Rocket Motor," AIAA Paper 86-1447, July 1986.

[24]Maicke, B. A., and Majdalani, J., "The Compressible Taylor Flow in Slab Rocket Motors," AIAA Paper 2006-4957, July 2006.

[25]Majdalani, J., and Vyas, A. B., "Inviscid Models of the Classic Hybrid Rocket," AIAA Paper 2004-3474, July 2004.